



Nanoscale

Ligand Accommodation Causes the Anti-centrosymmetric Structure of Au₁₃Cu₄ Clusters with Near-Infrared Emission

Journal:	<i>Nanoscale</i>
Manuscript ID	NR-ART-03-2020-002448.R2
Article Type:	Paper
Date Submitted by the Author:	14-May-2020
Complete List of Authors:	Anumula, Rajini; National Institute of Technology Warangal, Department of Chemistry Reber, Arthur; Virginia Commonwealth University, Physics An, Pan; Institute of Chemistry, Chinese Academy of Sciences Cui, Chaonan; Chinese Academy of Sciences, Institute of Chemistry Guo, Mengdi; Chinese Academy of Sciences, Institute of Chemistry Wu, Haiming; Institute of Chemistry, Chinese Academy of Sciences Luo, Zhixun; Chinese Academy of Sciences, Institute of Chemistry Khanna, Shiv; Virginia Commonwealth University, Physics Department

SCHOLARONE™
Manuscripts

ARTICLE

Ligand Accommodation Causes the Anti-centrosymmetric Structure of Au₁₃Cu₄ Clusters with Near-Infrared Emission

Rajini Anumula,^a Arthur C. Reber,^b Pan An,^a Chaonan Cui,^a Mengdi Guo,^a Haiming Wu,^a Zhixun Luo,^{*a} and Shiv. N. Khanna^{*b}

Received 00th January 20xx,
Accepted 00th January 20xx

DOI: 10.1039/x0xx00000x

We synthesized an [Au₁₃Cu₄(PPh₃)₄(SPy)₈]⁺ nanocluster co-capped by phosphine and thiolate ligands. Interestingly, this Au₁₃Cu₄ cluster corresponds to an anti-centrosymmetric structure with the four copper atoms coordinated to the mixed ligands on the same side of the Au₁₃ icosahedron, which is in sharp contrast to the [Au₁₃Cu₄(PPh₂Py)₄(SPhtBu)₈]⁺ and [Au₁₃Cu₂(PPh₃)₆(SPy)₆]⁺ clusters which possess highly symmetric structures with well-separated Cu adatoms. Both [Au₁₃Cu₄(PPh₃)₄(SPy)₈]⁺ and [Au₁₃Cu₂(PPh₃)₆(SPy)₆]⁺ clusters correspond to 8 valence electron superatoms with large HOMO-LUMO gaps, respectively. The difference in structure is rooted in the nature of the mixed ligands, with the bidentate SPy binding strongly to Cu on both binding sites (-N-Cu and Au-SR-Cu) leading to the co-linking of adjacent Cu atoms, while the bidentate PPh₂Py binds Cu on one site and Au on the other giving rise to a separation of the Cu atoms even in the presence of relatively higher monomer concentration. Both [Au₁₃Cu₄(PPh₃)₄(SPy)₈]⁺ and [Au₁₃Cu₂(PPh₃)₆(SPy)₆]⁺ display emissions in the near-IR regions. TD-DFT calculations reproduce the spectroscopic results with specified excited states, shedding light on the geometric and electronic behaviors of the ligand-protected Au₁₃M_x clusters.

Introduction

Clusters of thirteen metal atoms are often associated with high stability rationalized by their closed geometric and/or electronic shells.¹⁻⁷ In particular, the icosahedral Au₁₃ is a common structural motif in ligated clusters because when the cluster's effective valence count is eight electrons, the cluster has both highly stable geometric and closed electronic shells responsible for the enhanced stability.⁷⁻¹⁰ Extensive research efforts have culminated in the discovery of superatomic stability of M₁₃ clusters including Au_xM_{13-x},¹¹⁻¹³ and a 13-atom metal core is frequently embodied in ligand-protected M_{13+x} clusters, such as typical Au₂₅(SR)₁₈,¹⁴ Ag₂₅(SR)₁₈,¹⁵ [Cu₂₅H₂₂(PPh₃)₁₂]⁺,¹⁶ Au₁Ag₂₄(SR)₁₈,¹⁷ [Au₂Ag₄₂(SAdm)₂₇]⁺,¹⁸ as well as nanoclusters (NCs) like Au₁₉,¹⁹ Au₃₇,²⁰ Au₃₈,²¹ Au₆₀,²² Au₁₃₃,²³ Au₁₄₄,²⁴ Ag₂₁,²⁵ and Ag₁₅,²⁶ etc. Among these NCs, the metal clusters generally prefer a symmetric geometry to attain balanced charge distribution of the metallic core that minimizes energy. For example, recently Zheng et al.²⁷ synthesized an interesting class of bimetallic Au-Cu nanoclusters, where mixed ligands were employed to control the exposure of metallic sites

enabling regular capping of multiple copper atoms on balanced surface sites of the icosahedral Au₁₃ core.

However, there is no fundamental constraint for stable metal clusters to always form spherical structures, not only for noble metal clusters in gas phase,²⁸ but also metal NCs in the presence of alloy metals and mix ligands.²⁹ Theoretical advances on gas-phase metal clusters based on the Clemenger-Nilsson model allows for ellipsoidal distortion caused by Jahn-Teller effect,³⁰ enabling the electronic stability of metal clusters with non-magic numbers due to prolate or oblate deformations.^{30, 31} In wet chemistry, variation of ligands including halogens, phosphines, thiolates, selenolates, alkynes and amines could produce stable clusters with diverse geometry as a result of ligand engineering,³²⁻³⁶ against Mackay icosahedrons of closed geometric shells.^{37, 38} In particular, the interfacial structure between the metal core and the ligand could be different from each other in the presence of multiple ligands, especially those with unsaturated bonds, enabling new structures and properties of polymetallic nanoclusters.

While the stability of metal clusters is of significant research interest, in recent years the intrinsic photochemical properties of NCs have received increasing interest due to the advantages of their small particle sizes, biocompatible/degradable property, and controllability.³⁹ However, in most cases the photoluminescence of atomically precise nanoclusters is still unsatisfactory, not only the relatively low quantum yield, but also the emission lifetime and the emitted color is always red. Ongoing efforts are allowing one to address the shortcomings by ligand engineering and kernel alloying,⁴⁰⁻⁴⁵ endeavoring to attain a balance of external environment factors for better stability and better photoluminescent property.^{39, 46} For

^a Beijing National Laboratory for Molecular Sciences (BNLMS) and State Key Laboratory for Structural Chemistry of Unstable and Stable Species, and Key Laboratory of Photochemistry, Institute of Chemistry, Chinese Academy of Sciences, Beijing 100190, P.R. China. E-mail: zxlue@iccas.ac.cn

^b Department of Physics, Virginia Commonwealth University, Richmond, Virginia 23284, United States. Email: snkhanna@vcu.edu

* Correspondence. Emails: zxlue@iccas.ac.cn (Z.L.); snkhanna@vcu.edu (S.N.K.)

Electronic Supplementary Information (ESI) available: [details of Single Crystal data, experimental characterisation and DFT calculations.]. See DOI: 10.1039/x0xx00000x

example, several interesting studies have demonstrated dual luminescence⁴⁷ and NIR emissions with long lifetime,⁴⁸ indicating potentials in chemo-sensing and bio-imaging.^{48, 49}

In the present work, utilizing pyridyl-2-thiol and phosphine ligands, we have synthesized both $\text{Au}_{13}\text{Cu}_2(\text{SPy})_6(\text{PPh}_3)_6$ and $\text{Au}_{13}\text{Cu}_4(\text{SPy})_8(\text{PPh}_3)_4$ NCs under similar conditions with simply a different quantity of the copper salt. The two NCs with atomically precise and molecular purity were characterized by ESI-Mass spectrometry, single-crystal X-ray crystallography, as well as full spectroscopic studies. Interestingly, single crystals parsing shows that the former bears highly geometric structure with the two copper atoms located on two side. In contrast, $[\text{Au}_{13}\text{Cu}_4(\text{SPy})_8(\text{PPh}_3)_4]^+$ finds a different arrangement of copper atoms at the asymmetric sites and it exhibits interesting infrared luminescence showing long lifetime lasting up to microsecond, with remarkable stability for several months. DFT calculation results unveil the superatom cluster stability, electronic excited states and optical properties of this class of clusters, shedding light on the ligand accommodation in metal NCs by controlling the exposure and coordination of metal sites.

Fig. 1 presents the single-crystal structures of the as-synthesized $\text{Au}_{13}\text{Cu}_2$ and $\text{Au}_{13}\text{Cu}_4$ NCs. X-ray single crystal analysis reveals that $\text{Au}_{13}\text{Cu}_2$ and $\text{Au}_{13}\text{Cu}_4$ NCs are crystallized with orthorhombic and monoclinic packing structures with space groups of $Pmc2(1)$ and $P2_1/n$ respectively (Table S1, ESI). $\text{Au}_{13}\text{Cu}_2$ and $\text{Au}_{13}\text{Cu}_4$ NCs compositions were found to be $[\text{Au}_{13}\text{Cu}_2(\text{SPy})_6(\text{PPh}_3)_6]^+$ and $[\text{Au}_{13}\text{Cu}_4(\text{SPy})_8(\text{PPh}_3)_4]^+$ (Py = 2-pyridyl). Considering that electron transfer mainly occurs on -SPy group of thiols, both $\text{Au}_{13}\text{Cu}_2$ and $\text{Au}_{13}\text{Cu}_4$ NCs belong to 8-electron systems (simply, for $[\text{Au}_{13}\text{Cu}_4(\text{SPy})_8(\text{PPh}_3)_4]^+$: $N = 13 + 4 - 8 - 1 = 8$, while similarly for $[\text{Au}_{13}\text{Cu}_2(\text{SPy})_6(\text{PPh}_3)_6]^+$: $N = 13 + 2 - 6 - 1 = 8$). In view of this, both $\text{Au}_{13}\text{Cu}_2$ and $\text{Au}_{13}\text{Cu}_4$ NCs deserve their reasonable stability pertaining to superatom clusters with closed electronic shell structures.

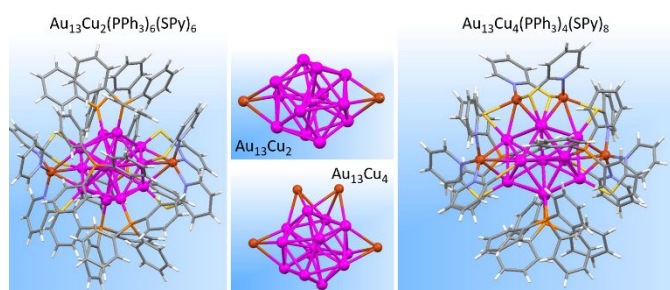


Fig. 1 The single-crystal structures of $[\text{Au}_{13}\text{Cu}_2(\text{SPy})_6(\text{PPh}_3)_6]^+$ and $[\text{Au}_{13}\text{Cu}_4(\text{SPy})_8(\text{PPh}_3)_4]^+$ clusters. Color legend for the cluster parts: violet sphere, Au; bronze sphere, Cu; light yellow sphere, S; orange sphere, P; grey stick, C; blue stick, N.

Interestingly, the single crystal structure analysis shows an anti-centrosymmetric geometry of the $\text{Au}_{13}\text{Cu}_4$ cluster with four copper atoms on the same side of Au_{13} icosahedron. Among the four Cu atoms, two are oriented on opposite sides of the cluster, face capping the Au_{13} core (forming spindle-shaped $\text{Au}_{13}\text{Cu}_2$) and triply coordinated to three nitrogen atoms of three pyridyl-2-thiol groups. The other two Cu atoms are asymmetrically

located on the same side of $\text{Au}_{13}\text{Cu}_2$, and triply coordinated to one nitrogen and two sulfur atoms of the pyridyl-2-thiol ligand. Two SPy ligands bridge the two equatorial Cu atoms, with one nitrogen site and one sulfur site bound to each copper atom, with a third bond formed with a neighboring SPy sulfur. This coordination of four Cu atoms in $[\text{Au}_{13}\text{Cu}_4(\text{SPy})_8(\text{PPh}_3)_4]^+$ differs from the previously reported $[\text{Au}_{13}\text{Cu}_4(\text{PPh}_2\text{Py})_4(\text{SPhBut})_8]$,²⁷ and $[\text{Au}_{13}\text{Cu}_4(\text{PPh}_2\text{Py})_3(\text{SePh})_9]$ clusters,⁵⁰ where the four Cu atoms are oriented in a tetrahedral geometry with the 4 Cu atoms equally and symmetrically spaced around the Au_{13} core. The copper atoms are exclusively triply coordinated to one nitrogen and two sulfur or selenium atoms of thiol and selenophenolate ligands.

The origin of anti-centrosymmetric geometry of the cluster $[\text{Au}_{13}\text{Cu}_4(\text{SPy})_8(\text{PPh}_3)_4]^+$, different from the literature report of $[\text{Au}_{13}\text{Cu}_4(\text{PPh}_2\text{Py})_4(\text{SC}_6\text{H}_4\text{-tert-C}_4\text{H}_9)_8]^+$ with a symmetric Au-Cu core,²⁷ is associated with the ligand itself. For the literature one, the PPh_2Py ligand bears both phosphine- and nitrogen- binding sites, allowing the phosphine binding to Au while the nitrogen bind to Cu,⁵¹ which helps the thiol ligand in stabilizing the metallic core with copper capping at balanced sites. While for $[\text{Au}_{13}\text{Cu}_4(\text{SPy})_8(\text{PPh}_3)_4]^+$ cluster in this study (details in Fig. S1, ESI), the bidentate SPy ligands have both a nitrogen site (that binds to Cu) and a thiol group (selectively bind to form an Au-S bond or an Au-S-Cu bond); meanwhile, the phosphine additive also binds weakly with the four uncapped Au atoms. Because of the existence of competition for the SPy ligands to form Au-S bonds or Au-S-Cu bonds, there comes a compromise solution by forming four Au-S bonds and four Au-S-Cu bonds respectively. In view of the steric hindrance of phosphine additive, and because the SPy ligand in this study is smaller in size than the ligands -SePh, - PPh_2Py and $\text{tert-C}_4\text{H}_9\text{-C}_6\text{H}_4\text{S-}$ in previous similar NCs, it is reasonable for the additional two copper atoms to be capped on the waist of the $\text{Au}_{13}\text{Cu}_2$. That is, the dramatic bidentate ligands give rise to a separation of Cu adatoms when using PPh_2Py and $\text{SC}_6\text{H}_4\text{-tert-C}_4\text{H}_9$, while a congregation of Cu adatoms in $\text{Au}_{13}\text{Cu}_4$ within the mixed PPh_3 and SPy protection.

In $[\text{Au}_{13}\text{Cu}_4(\text{SPy})_8(\text{PPh}_3)_4]^+$ clusters, the two oppositely oriented Cu atoms across Au_{13} core shows an average Au-Cu bond length at ~ 2.805 Å, while it is 2.859 Å for the two equatorially distributed Cu atoms. It is notable that, the Au-Au distances in the $\text{Au}_{13}\text{Cu}_4$ are averaged at 2.8034 Å, which is shorter than the Au-Au distance of bulk gold (~ 2.884 Å), indicating contraction of the $\text{Au}@\text{Au}_{12}$ core. Such an Au-Au bond contraction in $\text{Au}_{13}\text{Cu}_4$ clusters is due to subtraction of valence electrons by the electrophilic thiol ligands, and altered metal-metal interactions within the relativistic effect of gold.⁵²

The as-prepared $\text{Au}_{13}\text{Cu}_{2,4}$ NCs were further characterized by ESI-MS, as shown in Fig. 2. It is shown that a single intense and prominent peak observed at m/z 2453.78 and 2573.87 respectively, unambiguously corresponding to the molecular ions of $[\text{Au}_{13}\text{Cu}_2(\text{SPy})_6(\text{PPh}_3)_6]^+$ and $[\text{Au}_{13}\text{Cu}_4(\text{SPy})_8(\text{PPh}_3)_4]^+$, suggesting very high purity of the two NCs. The experimental isotopic and simulation patterns (Insets) are well consistent with each other.

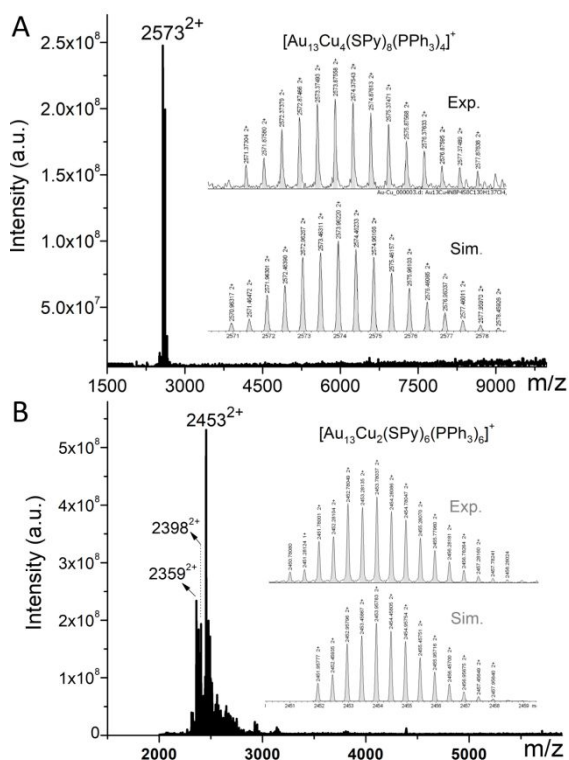


Fig. 2 ESI-MS of the as-prepared (A) $[\text{Au}_{13}\text{Cu}_4(\text{SPy})_8(\text{PPh}_3)_4]^+$ and (B) $[\text{Au}_{13}\text{Cu}_2(\text{SPy})_6(\text{PPh}_3)_6]^+$ clusters, collected in positive mode. The fragment peaks on the left correspond to the removal of a SPy group, and both a SPy and a benzene group. **Insets:** experimental and simulated isotopic patterns.

Fig. 3 shows the experimental and theoretical calculated UV-vis absorption spectra of $\text{Au}_{13}\text{Cu}_2$ and $\text{Au}_{13}\text{Cu}_4$ NCs. Interestingly the experimental UV-vis spectrum of $\text{Au}_{13}\text{Cu}_2$ NCs shows absorption bands at 475 and 575 nm, etc. Although a slight peak-position shift, this UV-vis spectrum substantially agrees with the previously published studies.^{27, 53} In comparison, the TD-DFT calculated UV-vis spectrum shows a few peaks assigned to molecule-like optical transitions, which is consistent with the experimental observation. For $\text{Au}_{13}\text{Cu}_4$ NCs, the experimental UV-vis absorption displays a wide absorption band up to 1000 nm along with three weak absorption peaks at 459, 520/555 nm. This experimental UV-vis spectrum of $\text{Au}_{13}\text{Cu}_4$ NCs shows accordance with the TD-DFT calculation results, but slightly different from that of the previously reported $[\text{Au}_{13}\text{Cu}_4(\text{PPh}_2\text{Py})_4(\text{SPhBut})_8]$ NCs.^{50,27} The absence of plasmonic absorption peak of gold NPs agrees with the anticipated optical transitions and suggest high purity of the as-synthesized NCs.

We then examined the emissions of the $\text{Au}_{13}\text{Cu}_2$ and $\text{Au}_{13}\text{Cu}_4$ NCs. The specialized near-infrared detector found a near-infrared emission peak at 965 nm for $[\text{Au}_{13}\text{Cu}_4(\text{PPh}_3)_4(\text{SPy})_8]^+$ (Fig. 4A), which is comparable with the DFT-calculated HOMO-LUMO gap of 1.17 eV. Similar results have also been found for the $\text{Au}_{13}\text{Cu}_2$ NCs which exhibit a NIR emission at 1006 nm, as shown in Fig. 4B. This is consistent with the DFT-calculated HOMO-LUMO energy gap of 1.23 eV for $[\text{Au}_{13}\text{Cu}_2(\text{PPh}_3)_6(\text{SPy})_6]^+$. It is worth mentioning that, the photoluminescence spectra by

a traditional spectrofluorometer showed that, for $\text{Au}_{13}\text{Cu}_4$ NCs, a near-infrared emission emerges at 818 nm (Fig. S4, ESI), which is similar to the previously reported studies.^{15, 50} For the $\text{Au}_{13}\text{Cu}_2$ NCs, a relatively weak emission was also observed at 815 nm, along with an emission band at visible region. Previously multicolor emissions of metal NCs have been frequently observed,^{47, 54-58} due to a synchronous fluorescence and phosphorescence, or a large gap between two electronically excited states enabling to suppress the internal conversion process hence radiative emission directly from the higher excitation states.

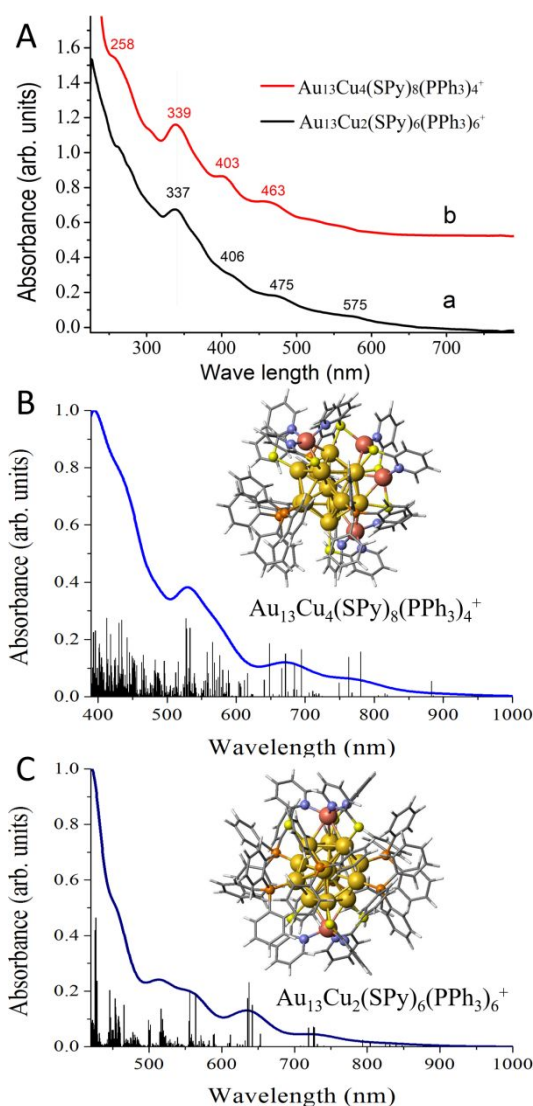


Fig. 3 A comparison of the experimental (red) and theoretical (blue) UV-vis absorption spectra of $[\text{Au}_{13}\text{Cu}_4(\text{SPy})_8(\text{PPh}_3)_4]^+$ (A) and $[\text{Au}_{13}\text{Cu}_2(\text{SPy})_6(\text{PPh}_3)_6]^+$ (B) clusters, respectively, measured in dichloromethane (DCM) solvent.

To better understand the novel emission of such NCs, we have performed a theoretical investigation into the electronic structure of the $\text{Au}_{13}\text{Cu}_2$ and $\text{Au}_{13}\text{Cu}_4$ clusters. Fig. 5 depicts the density of states and molecular orbitals of both the $[\text{Au}_{13}\text{Cu}_4(\text{PPh}_3)_4(\text{SPy})_8]^+$ and $[\text{Au}_{13}\text{Cu}_2(\text{PPh}_3)_6(\text{SPy})_6]^+$ clusters.

Note that, $[\text{Au}_{13}\text{Cu}_4(\text{PPh}_3)_4(\text{SPy})_8]^+$ has a large HOMO-LUMO gap of 1.17 eV and the electronic structure is that of an 8 valence electron cluster with an electronic structure of $1\text{S}^2|1\text{P}^6$, where the uppercase letters correspond to the symmetry of the delocalized orbital.

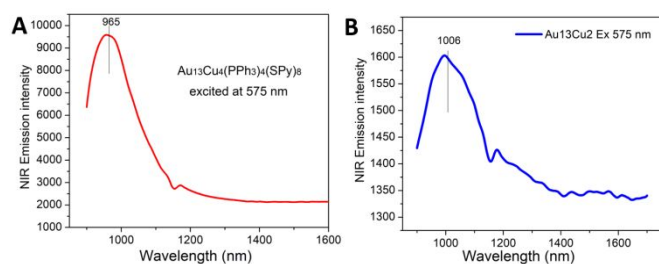


Fig. 4 Photoluminescence spectra of (A) $[\text{Au}_{13}\text{Cu}_4(\text{PPh}_3)_4(\text{SPy})_8]^+$ and (B) $[\text{Au}_{13}\text{Cu}_2(\text{PPh}_3)_6(\text{SPy})_6]^+$ clusters.

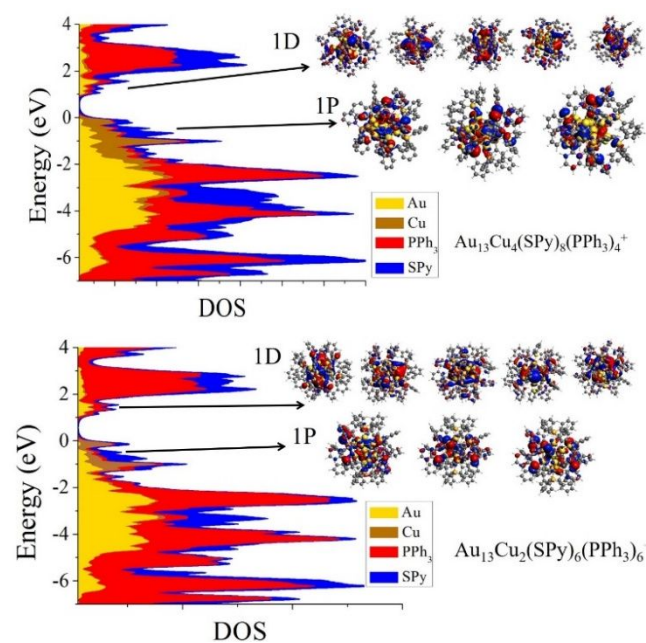


Fig. 5 Superatom analysis for the Kohn-Sham electron states of $[\text{Au}_{13}\text{Cu}_4(\text{SPy})_8(\text{PPh}_3)_4]^+$ and $[\text{Au}_{13}\text{Cu}_2(\text{SPy})_6(\text{PPh}_3)_6]^+$ clusters.

The molecular orbitals that correspond to the delocalized shell are also shown in Fig. 5, where the Cu atoms are found to be more positively charged than the Au atoms, with the average Hirschfeld charge on the Cu atoms being +0.19 |e| while the average charge on the Au atoms being +0.035 |e|. This is consistent with our argument that the reason for the anti-centrosymmetric structure is due to the nitrogen sites binding to the positively charge Cu preferentially than to the Au sites. The Mülliken population reveals that the 4s orbitals of the Cu atoms have an occupation of 0.36 |e| for the opposite Cu atoms and 0.51 |e| adjacent Cu atoms. The Mülliken population also reveals significant 4p occupation of the Cu atoms, a clear marker that the Cu should be considered metallic, rather than

considered to be in the +1 oxidation state.⁵⁹ The top of the filled valence electron band of the $[\text{Au}_{13}\text{Cu}_4(\text{PPh}_3)_4(\text{SPy})_8]^+$ cluster has significant Cu 3d occupation. The lowest energy unoccupied orbitals correspond to delocalized 1D^{10} orbitals. $[\text{Au}_{13}\text{Cu}_2(\text{PPh}_3)_6(\text{SPy})_6]^+$ is calculated to have a HOMO-LUMO gap of 1.23 eV, and also has an electronic shell structure that is consistent with that of an 8 valence electron superatom. The molecular orbitals are shown in Fig. 5. The Cu atoms in the $[\text{Au}_{13}\text{Cu}_2(\text{PPh}_3)_6(\text{SPy})_6]^+$ cluster are also found to be more positive than the Au atoms, with Hirschfeld charges found to be +0.19 |e| for Cu and 0.04 |e| for Au. The Mülliken population analysis reveals that the Cu atom has a 4p occupation of 0.69 |e|, which is relatively large and consistent with the fact that Cu atom is in a more metallic state comparing with its Cu^{+1} oxidation state.

In regards to the higher energy photoluminescence peaks in $[\text{Au}_{13}\text{Cu}_4(\text{PPh}_3)_4(\text{SPy})_8]^+$, we find the 10th, 11th and 12th excited states of $[\text{Au}_{13}\text{Cu}_4(\text{SPy})_8(\text{PPh}_3)_4]^+$ have large oscillator strengths. These three excitations correspond to 1P delocalized orbitals being excited to the 1D delocalized orbital, with energies of 1.59 eV, 1.62 and 1.63 eV corresponding to wavelength of 763-780 nm. Among them, the 11th excited state corresponds to an excitation from the HOMO of the cluster to top of the energy levels, suggesting that the fast-radiative emission could be a de-excitation from the 1D delocalized orbital to the 1P delocalized orbital. To some extent, this is consistent with the luminescence of the $\text{Au}_{13}\text{Cu}_4$ NCs in DCM solvent recorded by a traditional Horiba Scientific Fluoromax-4 spectrofluorometer (Fig. S4, ESI). We performed an optimization for the 10th excited state of $[\text{Au}_{13}\text{Cu}_4(\text{SPy})_8(\text{PPh}_3)_4]^+$, and found a photoluminescence energy of 1.39 eV corresponding to a wavelength of 892 nm. Therefore, the de-excitation of the 1D-1P superatomic transitions above the LUMO-HOMO de-excitation is likely responsible for the higher energy photoluminescence. We also note that the T_1 state is at 1.15 eV corresponding to a 1080 nm de-excitation, suggesting that higher energy emission is unlikely to be the T_1 - S_0 transition. Similar calculations have also been carried out for $[\text{Au}_{13}\text{Cu}_2(\text{SPy})_6(\text{PPh}_3)_6]^+$ where analogous excitations in this cluster are the 16-18th lowest excitations, with higher energies of 1.70-1.72 eV, or 720-727 nm. It is noteworthy that, these energies are calculated with no relaxation, thus should be higher than the experimentally obtained values.

Conclusions

We have successfully synthesized two Au-Cu alloy metal clusters, $[\text{Au}_{13}\text{Cu}_2(\text{PPh}_3)_6(\text{SPy})_6]^+$ and $[\text{Au}_{13}\text{Cu}_4(\text{PPh}_3)_4(\text{SPy})_8]^+$ by employing mixed ligands. The compositions of the $\text{Au}_{13}\text{Cu}_4$ and $\text{Au}_{13}\text{Cu}_2$ clusters were determined by ESI-MS spectrometry and single crystal X-ray crystallography. Both the two NCs are +1 charged and contain 8-electrons in its valence shell. The two clusters are found to be stable for up to several months showing reasonable stability of the 8-electron metallic cores and cooperative effect by the dual ligands of pyridine-2-thiol and triphenylphosphine. What is interesting is that, $\text{Au}_{13}\text{Cu}_2$ shows a symmetric structure with the two copper atoms located on two

triangular faces of icosahedral Au₁₃ from two ends, while Au₁₃Cu₄ bears an asymmetric structure pertaining to unusual Cu-capped kernel alloying process under the ligand engineering by mixed ligands. It is demonstrated that the cooperative effect of the mixed ligands could induce relatively less steric hindrance (or more Cu space occupancy) providing accessible sites for copper to be doped on neighboring surface sites from one side of the Au₁₃Cu₄ cluster. TD-DFT calculations reveal large HOMO–LUMO energy gaps at 1.17 eV and 1.23 eV for the two clusters, which are consistent with their reasonable stability pertaining to the nature of metal cluster core and ligand accommodation within variable steric hindrance and electrostatic interactions. Both Au₁₃Cu₄ and Au₁₃Cu₂ NCs display near-IR emission indicating potential applications in biosensing.

Materials and methods

Chemical reagents. Copper (II) acetate [Cu(OAc)₂, purity 99%] was purchased from Alfa Aesar Chemical Reagent; hydrogen tetrachloroaurate [HAuCl₄·4H₂O, purity 99.9%] from JK chemical company; sodium borohydride (NaBH₄, purity 98%) and triethylamine (C₆H₁₅N, A.R.) from Acros chemicals. Also, 2-pyridinethiol (C₅NH₅S, purity 99%) and triphenylphosphine (C₁₈H₁₅P, purity 95%) are from JK chemical company. Ultrapure Millipore water (18.2 MΩ·cm) was used for the synthesis and purification of nanoclusters. The solvents dichloromethane, methanol, ethanol, n-pentane, diethyl ether and n-hexane were of analytical grade of high purity and used without further purification.

Synthesis of precursor. Pure AuPPh₃Cl was synthesized from HAuCl₄·3H₂O and PPh₃ by the following procedures. Firstly, 1 g of HAuCl₄·3H₂O was dissolved in 80 mL absolute ethanol which was taken in a round-bottom flask. Then, 1.33 g of PPh₃ was dissolved in 40 mL ethanol which was then added to the above gold mixture under constant stirring. After stirring for about 30 min, white precipitates formed immediately and were filtered, washed with diethyl ether three times, and finally dissolved in CH₂Cl₂. Excess pentane was then added to the above solution to form white crystals of AuPPh₃Cl. All the above reaction steps were carried out at room temperature and in dark conditions as the synthesized AuPPh₃Cl is a light sensitive chemical.

Synthesis of Au₁₃Cu₄ clusters. The Au₁₃Cu₄ clusters were synthesized in one-pot by co-reduction of AuClPPh₃ and cupric acetate in presence of pyridine-2-thiol ligand by reducing with NaBH₄ in DCM and methanol solvents. Initially 12.36 mg Cu(OAc)₂ was taken in a round bottomed flask and was dissolved in methanol via ultrasonic assistance prior to the addition of AuPPh₃Cl. Later, 10 mg of the as-prepared AuPPh₃Cl precursor complex was dissolved in dichloromethane (DCM) solvent and added to the reaction mixture. The solution was cooled to 0 °C in an ice bath, and 7 mg 2-pyridinethiol dissolved in DCM was then directly added to the reaction mixture. After stirring for 20 minutes, 1 mL NaBH₄ aqueous solution (10 mg/mL) and 50 μL triethyl amine were added together quickly

to the reaction mixture under vigorous stirring. The reaction mixture was aged for 24 h at 0 °C. The aqueous phase was then removed using rotavapor and brown color extract were used for crystallization in CH₂Cl₂/hexane (1:4 ratio) solvents at 4 °C to afford black block crystals after 13 days. The yield of Au₁₃Cu₄ was up to ~40 %, and the washed clusters, stored in a freezer at 4 °C, were found to be highly stable for several months.

Synthesis of Au₁₃Cu₂ clusters. The synthesis of Au₁₃Cu₂ clusters is based on the literature method.²⁷ First, 12.0 mg Cu(OAc)₂ was dissolved in methanol and solubilized in help of ultrasonication. Next, similar procedures as above were conducted: 10 mg as-prepared AuPPh₃Cl was dissolved in DCM solvent and added to the above reaction mixture; the solution was kept in 0 °C ice bath; 7 mg 2-pyridinethiol dissolved in DCM was then added to the mixture; stirring for 20 minutes; 1 mL NaBH₄ aqueous solution (10 mg/mL) and 50 μL triethyl amine were added quickly together to the reaction mixture; and the solution was kept aging for 24 hours at 0 °C. The reaction mixture was then repeatedly washed with deionized water till it produces powder clusters. Black block crystals were crystallized from CH₂Cl₂/hexane at 4 °C after 10 to 15 days. The yield of the Au₁₃Cu₂ clusters was ~20%.

Characterization. The molecular formulas of ligand-protected Au₁₃Cu₂ and Au₁₃Cu₄ clusters were determined by single crystal parsing and confirmed by electron spray ionization mass spectrometry (ESI-MS). The Au₁₃Cu_x clusters were dissolved in DCM and mixed with methanol in the volume ratio of 1: 0.5 for ESI-MS measurements using a stainless-steel needle syringe. The instrument parameters used for the ESI-MS were kept in a mass range of 500–10000 Da, a capillary voltage of 3.0 kV, sample flow rate 120 μL/h, dry gas flow of 4.0 L/min at a temperature of 80°C, and the nebulizer gas pressure at 1.0 bar. The UV–vis absorption spectra were recorded using a Shimadzu UV-3600 UV-Vis-NIR spectrophotometer by dissolving the pure Au₁₃Cu_x crystals in DCM solvent. Photoluminescence spectra of the Au₁₃Cu_x clusters in DCM solvent were recorded by a normal Horiba Scientific Fluoromax-4 spectrofluorometer (PMT 200-950nm) and an Edinburgh FLS980 Fluorescence and lifetime spectroscopy (NIR PMT 900-1700nm), respectively. The fluorescence lifetime decay measurements were carried out on a spectra physics Millenia-eV with Tsunami laser, in DCM solvent.

Theoretical calculation methods. First-principles studies on the ligated clusters were carried out using Amsterdam Density functional (ADF) set of codes.⁶⁰ The generalized gradient approximation (GGA) of Perdew, Burke, and Ernzerhof (PBE) is used to incorporate the exchange and correlation effects.⁶¹ A TZ2P basis set and a large frozen electron core was used. The zero-order regular approximation (ZORA) is used to include scalar-relativistic effect.⁶² Time-dependent density functional theory (TD-DFT) was used to model the UV-Vis spectra, and the lowest 800 excitations were used.

Conflicts of interest

There are no conflicts to declare.

Acknowledgements

This work was financially supported by the Key Research Program of Frontier Sciences (CAS, Grant QYZDBSSWSLH024), and the National Natural Science Foundation of China (Grant No. 21722308; No. 21802146), by Beijing Natural Science Foundation (No. 2192064), by Frontier Cross Project of national laboratory for molecular sciences (No. 051Z011BZ3). Z. Luo acknowledges the National Thousand Youth Talents Program. S.N.K and A.C.R acknowledge the support from the Department of Energy (DOEAFOSR) through Grant DE-SC0006420n.

Notes and references

‡ CCDC 1971126 contains the supplementary crystallographic data for this paper. These data can be obtained free of charge from the Cambridge Crystallographic Data Centre via www.ccdc.cam.ac.uk/data_request/cif.

- D. E. Bergeron, A. W. Castleman, T. Morisato and S. N. Khanna, *Science*, 2004, **304**, 84-87.
- D. E. Bergeron, P. J. Roach, A. W. Castleman Jr., N. O. Jones and S. N. Khanna, *Science*, 2005, **307**, 231-235.
- R. Burgert, H. Schnöckel, A. Grubisic, X. Li and S. T. Stokes, *Science*, 2008, **319**, 438-442.
- Z. Luo and A. W. Castleman, *Acc. Chem. Res.*, 2014, **47**, 2931-2940.
- A. C. Reber and S. N. Khanna, *Acc. Chem. Res.*, 2017, **50**, 255-263.
- P. Jena and Q. Sun, *Super Atomic Clusters: Design Rules and Potential for Building Blocks of Materials*, 2018.
- Y. Jia and Z. Luo, *Coord. Chem. Rev.*, 2019, **400**, 213053.
- Y. Negishi, K. Nobusada and T. Tsukuda, *J. Am. Chem. Soc.*, 2005, **127**, 5261-5270.
- W. Ding, C. Huang, L. Guan, X. Liu, Z. Luo and W. Li, *Chem. Phys. Lett.*, 2017, **676**, 18-24.
- Z.-J. Guan, F. Hu, S.-F. Yuan, Z.-A. Nan, Y.-M. Lin and Q.-M. Wang, *Chem. Sci.*, 2019, 3360-3365.
- P. Pyykko and N. Runeberg, *Angew. Chem. Int. Ed.*, 2002, **41**, 2174-2176.
- Y. Shichibu and K. Konishi, *Small*, 2010, **6**, 1216-1220.
- M. Sugiuchi, Y. Shichibu, T. Nakanishi, Y. Hasegawa and K. Konishi, *Chem. Commun. (Cambridge, U. K.)*, 2015, **51**, 13519-13522.
- M. Zhu, C. M. Aikens, F. J. Hollander, G. C. Schatz and R. Jin, *J. Am. Chem. Soc.*, 2008, **130**, 5883-5885.
- C. P. Joshi, M. S. Bootharaju, M. J. Alhilaly and O. M. Bakr, *J. Am. Chem. Soc.*, 2015, **137**, 11578-11581.
- T. A. Nguyen, Z. R. Jones, B. R. Goldsmith, W. R. Buratto, G. Wu, S. L. Scott and T. W. Hayton, *J. Am. Chem. Soc.*, 2015, **137**, 13319-13324.
- M. S. Bootharaju, C. P. Joshi, M. R. Parida, O. F. Mohammed and O. M. Bakr, *Angew. Chem. Int. Ed.*, 2016, **55**, 922-926.
- S. Jin, X. Zou, L. Xiong, W. Du, S. Wang, Y. Pei and M. Zhu, *Angew. Chem. Int. Ed.*, 2018, **57**, 16768-16772.
- X. K. Wan, Q. Tang, S. F. Yuan, D. E. Jiang and Q. M. Wang, *J. Am. Chem. Soc.*, 2015, **137**, 652-655.
- R. Jin, C. Liu, S. Zhao, A. Das, H. Xing, C. Gayathri, Y. Xing, N. L. Rosi, R. R. Gil and R. Jin, *ACS Nano*, 2015, **9**, 8530-8536.
- W. T. E. Huifeng Qian, Yan Zhu, Tomislav Pintauer, and Rongchao Jin, *J. Am. Chem. Soc.*, 2010, **132**, 8280-8281.
- Y. Song, F. Fu, J. Zhang, J. Chai, X. Kang, P. Li, S. Li, H. Zhou and M. Zhu, *Angew. Chem. Int. Ed.*, 2015, **54**, 8430-8434.
- A. Dass, S. Theivendran, P. R. Nimmala, C. Kumara, V. R. Jupally, A. Fortunelli, L. Sementa, G. Barcaro, X. Zuo and B. C. Noll, *J. Am. Chem. Soc.*, 2015, **137**, 4610-4613.
- N. Yan, N. Xia, L. Liao, M. Zhu, F. Jin, R. Jin and Z. Wu, *Sci. Adv.*, 2018, **4**, 1-7.
- R. S. Dhayal, J. H. Liao, Y. C. Liu, M. H. Chiang, S. Kahlal, J. Y. Saillard and C. W. Liu, *Angew. Chem. Int. Ed.*, 2015, **54**, 3702-3706.
- X. T. Shen, X. L. Ma, Q. L. Ni, M. X. Ma, L. C. Gui, C. Hou, R. B. Hou and X. J. Wang, *Nanoscale*, 2018, **10**, 515-519.
- H. Yang, Y. Wang, J. Lei, L. Shi, X. Wu, V. Makinen, S. Lin, Z. Tang, J. He, H. Hakkinen, L. Zheng and N. Zheng, *J. Am. Chem. Soc.*, 2013, **135**, 9568-9571.
- J. Li, X. Li, H. J. Zhai and L. S. Wang, *Science*, 2003, **299**, 864-867.
- J. Yan, H. Su, H. Yang, C. Hu, S. Malola, S. Lin, B. K. Teo, H. Hakkinen and N. Zheng, *J. Am. Chem. Soc.*, 2016, **138**, 12751-12754.
- W. A. De Heer, *Rev. Mod. Phys.*, 1993, **65**, 611-676.
- M. Brack, *Rev. Mod. Phys.*, 1993, **65**, 677-732.
- C. Zeng, T. Li, A. Das, N. L. Rosi and R. Jin, *J. Am. Chem. Soc.*, 2013, **135**, 10011-10013.
- H. F. Qian, W. T. Eckenhoff, Y. Zhu, T. Pintauer and R. C. Jin, *J. Am. Chem. Soc.*, 2010, **132**, 8280-8281.
- Y. Shichibu, Y. Negishi, T. Watanabe, N. K. Chaki, H. Kawaguchi and T. Tsukuda, *J. Am. Chem. Soc.*, 2007, **111**, 7845-7847.
- T. Iwasa, K. Nobusada and A. Nakajima, *J. Phys. Chem. C*, 2013, **117**, 24586-24591.
- M. Walter, J. Akola, O. Lopez-Acevedo, P. D. Jadzinsky, G. Calero, C. J. Ackerson, R. L. Whetten, H. Groenbeck and H. Hakkinen, *Proc. Natl. Acad. Sci. U. S. A.*, 2008, **105**, 9157-9162.
- X. K. Wan, X. L. Cheng, Q. Tang, Y. Z. Han, G. Hu, D. E. Jiang and Q. M. Wang, *J. Am. Chem. Soc.*, 2017, **139**, 9451-9454.
- N. A. Sakthivel, S. Theivendran, V. Ganeshraj, A. G. Oliver and A. Dass, *J. Am. Chem. Soc.*, 2017, **139**, 15450-15459.
- S. S. Zhang and M. Zhu, *Chem. Soc. Rev.*, 2019, **48**, 2422-2457.
- Q. Yao, Y. Feng, V. Fung, Y. Yu, D. E. Jiang, J. Yang and J. Xie, *Nat. Commun.*, 2017, **8**, 1555.
- O. Fuhr, S. Dehnen and D. Fenske, *Chem. Soc. Rev.*, 2013, **42**, 1871-1906.
- M. S. Bootharaju, S. M. Kozlov, Z. Cao, M. Harb, N. Maity, A. Shkurenko, M. R. Parida, M. N. Hedhili, M. Eddaoudi, O. F. Mohammed, O. M. Bakr, L. Cavallo and J. M. Basset, *J. Am. Chem. Soc.*, 2017, **139**, 1053-1056.
- I. Chakraborty and T. Pradeep, *Chem Rev*, 2017, **117**, 8208-8271.
- S. Li, X. S. Du, B. Li, J. Y. Wang, G. P. Li, G. G. Gao and S. Q. Zang, *J. Am. Chem. Soc.*, 2018, **140**, 594-597.
- S. S. Zhang, F. Alkan, H. F. Su, C. M. Aikens, C. H. Tung and D. Sun, *J. Am. Chem. Soc.*, 2019, **141**, 4460-4467.
- T. Higaki, Q. Li, M. Zhou, S. Zhao, Y. Li, S. Li and R. Jin, *Acc. Chem. Res.*, 2018, **51**, 2764-2773.
- R. W. Huang, Y. S. Wei, X. Y. Dong, X. H. Wu, C. X. Du, S. Q. Zang and T. C. W. Mak, *Nat Chem*, 2017, **9**, 689-697.
- X. K. Wan, W. W. Xu, S. F. Yuan, Y. Gao, X. C. Zeng and Q. M. Wang, *Angew. Chem. Int. Ed.*, 2015, **54**, 9683-9686.
- Q. Li, M. Zhou, W. Y. So, J. Huang, M. Li, D. R. Kauffman, M. Cotlet, T. Higaki, L. A. Peteanu, Z. Shao and R. Jin, *J. Am. Chem. Soc.*, 2019, **141**, 5314-5325.
- Y. Song, Y. Lv, M. Zhou, T. Y. Luo, S. Zhao, N. L. Rosi, H. Yu, M. Zhu and R. Jin, *Nanoscale*, 2018, **10**, 12093-12099.

51. A. C. Reber, D. Bista, V. Chauhan and S. N. Khanna, *J. Phys. Chem. C*, 2019, **123**, 8983-8989.
52. V. W.-W. Yam, *Angew. Chem. Int. Ed.*, 2000, **39**, 1683-1685.
53. C. Zhou, H. Li, Y. Song, F. Ke, W. W. Xu and M. Zhu, *Nanoscale*, 2019, **11**, 19393-19397.
54. Q.-Q. Xu, X.-Y. Dong, R.-W. Huang, B. Li, S.-Q. Zang and T. C. Mak, *Nanoscale*, 2015, **7**, 1650-1654.
55. Z. Lei, Z. J. Guan, X. L. Pei, S. F. Yuan, X. K. Wan, J. Y. Zhang and Q. M. Wang, *Chem. - Eur. J.*, 2016, **22**, 11156-11160.
56. Z. Lei, Z. J. Guan, X. L. Pei, S. F. Yuan, X. K. Wan, J. Y. Zhang and Q. M. Wang, *Chemistry*, 2016, **22**, 11156-11160.
57. G. Brancato, G. Signore, P. Neyroz, D. Polli, G. Cerullo, G. Abbandonato, L. Nucara, V. Barone, F. Beltram and R. Bizzarri, *J. Phys. Chem. B*, 2015, **119**, 6144-6154.
58. R. Anumula, P. Xiao, C. Cui, H. Wu, G. Cui, W.-h. Fang, Z. Luo and J. Yao, *Nanoscale*, 2020, **12**, 7864-7869.
59. C. J. Grover, A. C. Reber and S. N. Khanna, *J. Chem. Phys.*, 2017, **146**, 224301.
60. G. te Velde, F. M. Bickelhaupt, E. J. Baerends, C. Fonseca Guerra, S. J. A. van Gisbergen, J. G. Snijders and T. Ziegler, *J. Comput. Chem.*, 2001, **22**, 931-967.
61. J. P. Perdew, K. Burke and M. Ernzerhof, *Phys. Rev. Lett.*, 1996, **77**, 3865-3868.
62. E. v. Lenthe, E. J. Baerends and J. G. Snijders, *J. Chem. Phys.*, 1994, **101**, 9783-9792.

TOC Graphic

